Camera-based Methodology for the Automated Real-Time Assessment of Material Thinning in Battery Cell Manufacturing

Florens Wurmer[1](✉), Niklas Kesten[1], Matthias Burgard[1], Marcel Daumüller[1], and Florian Maier[1]

[1]Fraunhofer Institute for Manufacturing Engineering and Automation IPA, Nobelstraße 12, 70569 Stuttgart, Germany
{florens.wurmer, niklas.kesten, matthias.burgard, marcel.daumueller, florian.maier}@ipa.fraunhofer.de
https://www.ipa.fraunhofer.de/en.html

Abstract. As global demand for electric vehicles and energy storage systems increases, the design and manufacturing of electrochemical batteries play a crucial role in meeting these needs. However, evolving cell designs and high safety requirements pose significant challenges in mass production, leading to high scrap rates and increased energy consumption. Traditional methods for examining the cell interior, such as CT scans and X-rays, are costly and often allow only random quality inspections, resulting in further manufacturing scrap. To address this, we present a method for non-destructive inline measurement of battery case wall thickness during the assembly of cylindrical cells, utilizing a calculation model and an industrial camera system. After the forming process, cell cases are automatically measured and evaluated for critical wall thickness using our model, which is integrated into the machine control system for efficient quality assessment. Our research successfully demonstrates the indirect determination of material thinning through camera-based methods, establishing a correlation between our quality assessment results and experimentally validated product quality, with a Pearson correlation coefficient of 0.94, indicating a strong linear correlation in our evaluated data. This publication presents a novel approach for inline 100% inspection of material thinning during the shaping of cylindrical battery cases, minimizing the reliance on CT scans and X-rays. This method offers significant advantages in production costs, product quality, and sustainability, and can also be applied to other manufacturing processes involving the high-precision reshaping of metallic materials.

Keywords: Battery Cell Manufacturing · Cylindrical Battery Cells · Spin Groove Forming · Non-Destructive Testing · Wall Thickness Measurement

The final publication is available at Springer via http://dx.doi.org/10.1007/978-3-032-03546-2_24

1 Introduction

1.1 Topic Relation

In recent years, the increasing progress in electric vehicle manufacturing and renewable energy solutions has underscored the critical role of lithium-ion battery cells as a key technology. As the demand for efficient energy storage and sustainable power sources escalates, the manufacturing of these battery cells has become paramount. Consequently, advancements in lithium-ion battery technology and production processes are essential to meet the growing market needs and enhance battery performance, lifespan, and affordability [1].

In the competitive landscape of mass battery production, automotive manufacturers and battery cell producers are exploring prismatic, pouch, and cylindrical cell designs, each serving distinct applications. Recently, there has been a notable shift towards cylindrical cells for electric vehicle use. The most prevalent and extensively researched cylindrical cell designs include the 18650, 21700, and 4680 formats [2-4].

With the rapid development of new and improved cell designs, there is also a need for the innovation and advancement of the required production technologies. Consequently, numerous engineering companies are currently investing in the construction of new gigafactories and optimizing individual production processes for the manufacture of lithium-ion cylindrical cells. However, this highly dynamic evolution of production facilities is associated with high scrap rates. Companies aiming to produce large amounts of battery cells in the future typically generate a significant amount of waste, which then must be disposed of, leading to considerable energy and material wastage. Given that material costs account for approximately 65 to 80 percent of the manufacturing costs in lithium-ion battery production, this issue is seen as highly problematic [4]. Therefore, minimizing production waste is an essential tool for achieving a more sustainable and cost-efficient mass production of energy storage systems in the future [5].

High manufacturing scrap rates are not only a result of suboptimal production processes but are also caused by the potential safety risks associated with poorly manufactured battery cells. Increased charging and discharging speeds, along with the ever-growing demands on vehicle batteries, heighten the risk of fires in electric vehicles. The spontaneous ignition of batteries can often be attributed to unsuitable production processes, highlighting the critical importance of highly accurate quality control at nearly every step of the battery production process [6].

Next-generation lithium-ion battery cell designs feature enhanced specific energy, which further intensifies the severity of thermal runaway safety risks. Thermal runaway propagation in battery cell packs can cause adjacent cells to experience similar failures, as demonstrated in the setup described in [7]. It begins when a single cell overheats, often due to factors like overcharging or internal short circuits. This overheating generates heat and may release gases, raising the temperature of nearby cells. If not contained, this process can escalate, resulting in multiple cells failing in succession. The cumulative effect can lead to

The final publication is available at Springer via
http://dx.doi.org/10.1007/978-3-032-03546-2_24

fire, smoke, or even explosion, making thermal runaway propagation a significant safety concern in battery pack design. One way to reduce the risk of thermal runaway propagation in lithium-ion battery packs, which can be incorporated into the manufacturing process, is to minimize the risk of spin groove ruptures in the individual cells. This can be achieved by reliably maintaining the maximum possible wall thickness of the battery case, also known as the battery can [7].

To detect spin groove ruptures and other quality defects that can occur within the cell casing, traditional X-ray or CT-scan methods are used, which allow a view into the interior of the cells. However, a disadvantage of these processes is that they are time-consuming and are therefore mostly used in the form of production-related random sampling measurements. To ensure 100% inspection that can keep up with the high cycle times of mass production, existing methods must be further developed or new methods must be created [8].

We propose the hypothesis that there is a measurable correlation between material thinning occurring in the production process within the spin groove and the calculable extent of material stretching due to the grooving process, which opens up new possibilities for rapid and non-destructive quality testing.

1.2 Motivation

To optimize existing and future mass production plants for cylindrical lithium-ion battery cells, we propose a methodology for determining material thinning during the assembly of these cells. Our approach aims to implement a 100% inline quality checking process to reduce scrap cells and enhance the efficiency of the assembly process while also consuming less energy, thereby achieving greater sustainability. Instead of relying on traditional methods for measuring the thickness of cell cans, such as CT scans and polished cross section images, our approach utilizes conventional industrial camera systems combined with a physical calculation model to determine the wall thickness of the metal cans. This enables a more cost-effective process that can keep pace with the high cycle times essential for profitable mass production of battery cells.

1.3 Paper Structure

In Chapter 2, we begin by evaluating existing approaches for checking the geometry and wall thickness of battery cans during the mass production of cylindrical battery cells. Following this, we provide an overview of established methods for calculating material thinning in metal forming, based solely on the outer measurements of the processed metals. Next, in Chapter 3, we describe our approach, including the necessary hardware and software components required to implement the system in a manufacturing plant. Our methods are then evaluated in Chapter 4, using data generated during our research. Key findings and the practical applicability for the industry are summarized at the end in Chapter 5, highlighting the benefits that can be achieved by utilizing the introduced system.

The final publication is available at Springer via
http://dx.doi.org/10.1007/978-3-032-03546-2_24

2 Related Work

X-ray imaging plays a crucial role in the production of lithium-ion batteries by enabling non-destructive testing of critical internal features within an inline measurement, which enhances overall quality control. This technology allows for the detection of defects early in the manufacturing process, thereby preventing defective materials from progressing through the production line, ultimately increasing efficiency and safety. The primary advantage of X-ray imaging is its non-destructive nature, allowing for the examination of internal features without damaging the components. This technique can identify defects such as air pockets or material inconsistencies. On the other side, X-ray imaging has its limitations. The inspection can be time-consuming, especially when high-resolution images are required, which may not be suitable for high-speed production lines. Moreover, certain X-ray techniques may require extensive sample preparation, making them less practical for inline applications. Another disadvantage is the resolution constraints. While it can reveal significant defects, it may not capture finer details compared to other techniques. In summary, while X-ray imaging is an effective tool for detecting defects in battery production, its limitations in resolution and speed should be considered when selecting inspection techniques [8].

While X-ray imaging provides a valuable means of detecting defects in production through non-destructive testing, X-ray computed tomography (CT) takes this a step further by offering detailed three-dimensional visualizations that enhance the understanding of internal structures and relationships within an object.

X-ray computed tomography (CT) operates by using X-rays to penetrate an object, capturing the transmitted radiation to create two-dimensional images, which are then processed using reconstruction algorithms to generate detailed three-dimensional visualizations. It has become an essential tool for detecting defects in lithium-ion batteries, offering both positive and negative impacts on the manufacturing process. CT offers a non-destructive method to visualize the internal structures of batteries three-dimensionally. It allows the identification of defects that could lead to battery failure or safety issues and the identification of structural deformations without disassembly. This capability allows for the inspection of all produced cells, which is a requirement in industrial production to ensure quality and safety. The advantages of CT technology include high resolution, providing detailed images of small internal features, and the ability to conduct inspections without damaging the battery. It can effectively assess various components, including electrode materials and assembly integrity, enabling manufacturers to enhance quality control and optimize production processes. However, there are also challenges associated with the use of CT scans in battery production. CT imaging can be time-consuming and by this be a bottleneck in the production process, potentially slowing down the overall manufacturing speed. Additionally, the effectiveness of CT may be limited by the physical properties of battery casing materials, which can attenuate X-ray signals and reduce image clarity. In summary, while CT technology significantly enhances the detection of defects in battery cells and supports the development of safer, more

The final publication is available at Springer via
http://dx.doi.org/10.1007/978-3-032-03546-2_24

reliable batteries, it also faces challenges related to imaging speed and material compatibility [9].

To detect certain defect patterns in cell production without the use of X-rays and CT scans, efforts are being made to address quality risks such as material thinning with other non-destructive measuring methods. Material thinning during forming processes refers to the reduction in thickness of sheet materials as they are shaped into components. This issue is critical in the metal forming industry, as excessive thinning can lead to structural failures, such as cracks. The detection of material thinning is essential to ensure product quality and prevent defects. A problem is that the complexity of the forming process can make it challenging to predict thinning accurately, especially when multiple variables are at play. To address this, non-destructive testing methods like eddy current testing can be employed. Eddy current testing utilizes electromagnetic induction to detect flaws in conductive materials by inducing eddy currents within the material. This technique is particularly effective in identifying material thinning and cracks, providing valuable insights during the manufacturing process. However, there are some disadvantages to consider. Different materials will produce varying responses during eddy current testing, which can complicate the interpretation of results. Additionally, a high level of expertise is necessary for the teach-in process, as operators must be skilled in calibrating the equipment and understanding the results [10].

Another way to achieve non-contact quality control is through optical measurement methods, which are crucial in dimensional metrology within production due to their ability to provide fast and accurate measurements. These methods utilize light to measure dimensions. They are particularly suitable for integration into production lines, offering the potential for automation and real-time quality control. Given the evolving demands for precision and reliability, optical methods can acquire much data in a shorter time frame. The advantages of optical measurement methods include non-contact measurement, which minimizes the risk of damaging sensitive parts, and the ability to integrate these methods into production lines for real-time monitoring. Optical systems can achieve high resolutions, with some technologies reaching down to the nanometer scale. A disadvantage of optical measurement systems can be the sensitivity to environmental conditions such as temperature, vibrations and contamination, which can affect measurement accuracy. Moreover, the complexity of interpretation and the reliance on specific surface properties can present challenges. For example, measurements can be affected by the reflectivity and texture of the surfaces being evaluated. In summary, while optical measurement methods offer significant benefits for dimensional metrology in production, there are challenges related to environmental sensitivity and data interpretation [11].

3 Methodology and System Design

To achieve a 100% inspection of wall thickness and potential material thinning, our methodology follows a systems engineering approach, which focuses on the

The final publication is available at Springer via
http://dx.doi.org/10.1007/978-3-032-03546-2_24

holistic integration of hardware and software components to achieve optimal results. Each phase of our research process is designed in a way that allows the results to work together efficiently in the emerging system. We begin with the selection of a mass production-compatible vision system, which is intended to capture the outer dimensions of the reshaped cell cans after the formation of the spin groove. This is followed by the acquisition and transfer of the necessary data. The measurements are then incorporated into a calculation model that determines the extent of any material thinning present in the spin groove. The knowledge gained about the calculated wall thickness in the spin groove of each cell can subsequently be used to filter out cans of insufficient quality and to plan early maintenance of the production machines. Through this approach, we aim to direct our research efforts toward the development of a system that can be of practical use in real-world manufacturing environments. The individual elements of this system will be described in detail below.

3.1 Data Collection

The collection of data required for the calculation model must be carried out using an industrial measurement system capable of maintaining a high cycle time. For the subsequent use of the recorded data, it is also important that the device has a suitable software interface that enables seamless communication with the plant control system. Several manufacturers produce sensor technology that offers measuring devices for such applications. For our approach, we selected a state-of-the-art double-telecentric optical system specifically designed for various industrial applications, including automation, quality control, inspection, and identification. This system features a high-resolution CMOS image sensor, providing a resolution of 1920 x 1080 pixels for detailed image capture. It enables measurement speeds as rapid as 3 ms, with an accuracy of $\pm$ 2.5 μm. Additionally, it supports straightforward connectivity via common industrial communication interfaces, facilitating seamless integration into existing systems. These features made it the preferred choice over other available systems. Refer to [12] for more information about the described vision system.

For the calculation of material thinning, the sensor must capture relevant external geometric dimensions. This includes the bending radii of the spin groove as well as the distances between the individual radii. Ideally, a complete cell is measured in cross-section. However, in industrial production systems, there is typically the challenge that cell cans are processed through individual production stages in workpiece carriers, so that only a portion of the cell can is visible to the sensor. Fig. 1 illustrates two scenarios of data acquisition with the Vision System: on one hand, the measurement of the entire cell and, on the other hand, the measurement of the cell within a workpiece carrier.

To ensure mass production applicability, we examine the determination of material thinning with a measurement field that covers the complete battery can (see Fig. 1, left) as well as a limited measurement field (see Fig. 1, right). The recorded measurement data is stored in real-time by the measurement device's

The final publication is available at Springer via
http://dx.doi.org/10.1007/978-3-032-03546-2_24

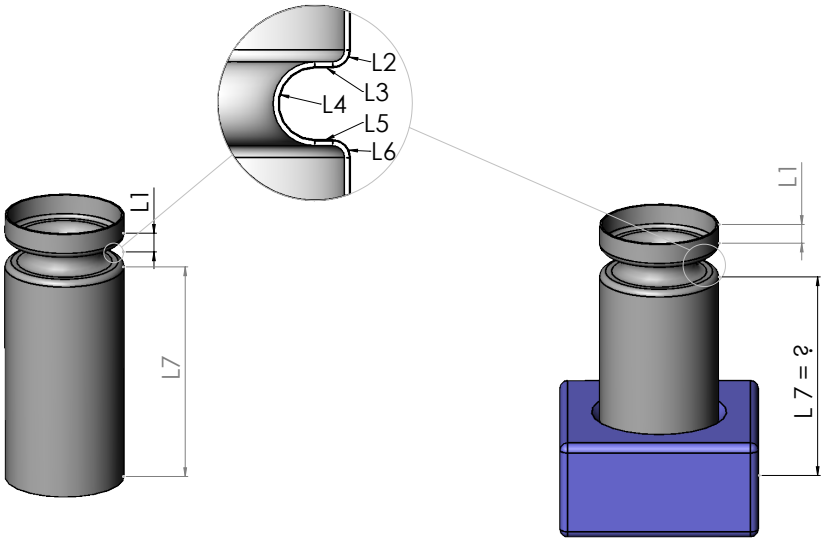

Fig. 1. Representation of the battery can to be measured. Left: complete can, Right: partially obscured can in workpiece carrier.

control unit directly on the plant's control computer via an EtherCAT interface during ongoing production, allowing for further utilization there.

3.2 Automated Data Analysis

The automated analysis of the geometric measurement data captured during the process will be carried out using a calculation model that aims to provide an estimate of the wall thickness of each processed cell. The calculation model is based on the principle of the stretched length, which already finds extensive application in the field of sheet metal forming. The stretched length refers to the length of a sheet metal piece required after deformation to achieve a specific geometry. It is crucial for the planning and calculation of forming processes, as it takes into account how the material is stretched during deformation. The stretched length corresponds to the length of the neutral fiber of a bent part, which is the area within a material that is neither stretched nor compressed during a bending process. The calculation of the neutral fiber, and thus the stretched length referred to as L, can be performed using the following formulas [13]:

$$L_F = L_1 + L_2 + L_3 + L_4 + L_5 + L_6 + L_7 \tag{1}$$

$$L = d_m \cdot \pi \cdot \frac{\alpha}{360°} \tag{2}$$

$$d_m = D - s = d + s \tag{3}$$

In this context, L_F represents the stretched length of the free-standing can and L_1 to L_7 indicate the partial lengths of L_F. If a partial length corresponds

The final publication is available at Springer via
http://dx.doi.org/10.1007/978-3-032-03546-2_24

to a straight section, only the length of that section is considered. If it is a curved section, formula (2) is applied. The mean diameter d_m can be calculated by adding or subtracting the thickness s from the inner diameter d or outer diameter D of the curved section. The bend angle α is the angle between the original and bent sections of a material.

As evident from the formulas, only the diameter, the original wall thickness and the angle of the bent sections of the bending part are required. We utilize this concept in our approach for battery cell production to estimate the height that the battery can would need to have before the forming process, assuming ideal forming without any stretching or compression of the material. This calculated value can then be compared with the actual can height of the processed cells before they were formed. Since battery cans used in mass production are generally purchased components that undergo incoming goods inspection, the height of the formed cans can be obtained from the corresponding data sheet.

Using formulas (1) to (3) and the partial lengths shown on the left in Fig. 1, the stretched length of the free-standing battery can L_F is calculated as follows:

$$\begin{aligned} L_F &= L_1 + \frac{d_{m,L_2} \cdot \pi \cdot \alpha_{L_2}}{360^\circ} + L_3 + \frac{d_{m,L_4} \cdot \pi \cdot \alpha_{L_4}}{360^\circ} + L_5 + \frac{d_{m,L_6} \cdot \pi \cdot \alpha_{L_6}}{360^\circ} + L_7 \\ &= L_1 + \frac{(D_{L_2} - s) \cdot \pi \cdot 90^\circ}{360^\circ} + L_3 + \frac{(d_{L_4} + s) \cdot \pi \cdot 180^\circ}{360^\circ} + L_5 + \frac{(D_{L_6} - s) \cdot \pi \cdot 90^\circ}{360^\circ} + L_7 \\ &= L_1 + \frac{(D_{L_2} - s) \cdot \pi}{4} + L_3 + \frac{(d_{L_4} + s) \cdot \pi}{2} + L_5 + \frac{(D_{L_6} - s) \cdot \pi}{4} + L_7 \end{aligned} \quad (4)$$

Since the used measuring device can only reproduce the radii but not the exact arc lengths of the radii r_{L_2}, r_{L_4}, and r_{L_6} in an automated manner, it is assumed based on the desired target geometry of the battery can that α_{L_2} and α_{L_6} are 90 degrees and α_{L_4} is 180 degrees. This assumption is acceptable because our proposed calculation model is based on the relationship between the stretched length and the wall thickness, rather than the absolute values of each individual segment of the cell can.

The comparison of the calculated stretched length, representing an ideal bending process, with the actual length of the can specified in the corresponding data sheet, referred to as $L_{original}$, provides information about the deviation of the actual bending from the ideal bending, as shown in (5). If the calculated stretched length is greater than the actual length, this indicates that material thinning has occurred. If the calculated and actual lengths are equal, it indicates that an ideal bending process has taken place, and thus no material thinning has occurred.

$$\text{Material Thinning} = \begin{cases} \text{existent} & \text{if } L_F > L_{original} \\ \text{non-existent} & \text{if } L_F = L_{original} \end{cases} \quad (5)$$

To use this method in mass production with workpiece carriers, we also investigated whether it is possible to make a statement about the material thinning

The final publication is available at Springer via
http://dx.doi.org/10.1007/978-3-032-03546-2_24

by considering only the partial lengths L_2, L_4 and L_6. For this purpose, we calculate a reduced form of the stretched length that addresses the use of workpiece carriers, referred to as L_{WC}, using the following formula:

$$L_{WC} = \frac{(D_{L_2} - s) \cdot \pi}{4} + \frac{(d_{L_4} + s) \cdot \pi}{2} + \frac{(D_{L_6} - s) \cdot \pi}{4} \tag{6}$$

Apart from the ability to determine whether material thinning occurs, we also aim to assess the extent of material thinning with our approach. We propose the hypothesis that an increased difference between L_F and $L_{original}$ is linearly correlated with the thinning of the material. Also we assume, that there is likewise a linear correlation between L_{WC} and thinning of the material.

To infer the wall thickness of the can, a dataset of cell cans with varying degrees of material thinning is created. After measuring the relevant geometric features of the cans, these are processed into cross-sectional images, allowing for the actual material thinning of the cans to be measured using a microscope.

A comparison can now be made between the data captured by the optical measurement system and the data obtained from cross-sectional images. If a correlation is found between L_F/L_{WC} and the minimum wall thickness, this approach can assess material thinning solely through optical measurements during production, eliminating the need for destructive methods like creating cross-sectional images. To calculate a specific value for material thinning, linear interpolation of the two measurement datasets can be performed, resulting in a relationship of material thinning MT as a function of the calculated stretched length $L_{(F/WC)}$, as shown in formula (7) [14]:

$$MT(L_{(F/WC)}) = MT_i + \frac{(MT_{i+1} - MT_i)(L_{(F/WC)} - L_{(F/WC),i})}{(L_{(F/WC),i+1} - L_{(F/WC),i})} \tag{7}$$

The resulting equation for determining material thinning, along with all necessary preliminary calculations, is implemented in the control software of the overall system. This system consists of an industrial computer (Beckhoff C6030-0060) and the previously described vision system (see [12]). The vision system communicates with the industrial computer via the real-time EtherCAT protocol over a wired connection. To capture the geometric features shown in Fig. 1, a corresponding measurement program is created using the operator software of the vision system, which is executed by the connected industrial computer. The calculations presented in formulas formulas (1) to (7) are implemented as a software module in Structured Text (ST) and deployed as a runtime file on the industrial computer. The use of the EtherCAT protocol ensures deterministic communication with cycle times below 10 ms. This setup enables the described calculation model to be executed in real time during battery cell production, allowing for immediate warnings or ejection of cells with dangerously high material thinning and facilitating early responses to process changes that could negatively impact product quality.

The final publication is available at Springer via
http://dx.doi.org/10.1007/978-3-032-03546-2_24

4 Evaluation

To validate our proposed system, we will create a dataset consisting of partially assembled battery cell cans. These cans will first be measured automatically according to the principles described in Chapter 3 and analyzed through our calculation model. As a result, we obtain a value for the degree of material thinning for each cell can, which must then be verified for its correctness. To do this, the processed and measured cell cans will be embedded in a curing compound and subsequently cut in half, allowing the wall thickness to be accurately measured under a microscope. The comparison of these destructive measurements with the results of our calculation model will ultimately provide insights into how accurately the system works.

The battery can material that has been used is a cold-rolled, low-carbon steel with deep-drawing quality, selected for its excellent formability and mechanical strength. This steel exhibits a typical yield strength in the range of 210–325 MPa and a tensile strength of 290–390 MPa, with elongation at break above 24%. Both the interior and exterior surfaces of the cans are coated with a nickel layer, with a thickness of up to 4 μm, to enhance corrosion resistance and ensure chemical compatibility with the battery components.

To create the dataset for testing the system, six different parameter configurations for the setting of the spin grooving machine were employed, leading to varying degrees of material thinning in the spin groove. These parameter configurations are referred to as Configuration A, B, C, D, E, and F. During the spin grooving process, the axial stroke, which influences the material's flow behavior during bending, was iteratively reduced by 0.2 mm for each parameter configuration starting with A and ending with F, theoretically increasing the occurrence of material thinning in descending order. The axial stroke in our experiment was achieved using a pneumatic cylinder operated at a pressure of 3 bar. It can therefore be assumed that Configuration A results in the least and Configuration F in the greatest extent of material thinning. Further reducing the axial stroke beyond what is present in Configuration F leads to clearly visible cracks and destruction of the battery can, which is why Configuration F can be described as the worst-case scenario regarding the adjustment of the machine parameters.

To produce statistically significant results, 10 battery cans were processed with each parameter configuration. These were then measured using the vision system. Subsequently, the measurement data were used with our calculation model to determine the calculated stretched lengths L_F and L_{WC}. For the value of the actual can length, the value from the corresponding datasheet of the purchased cans was used, which specifies a can height of 73 ± 0.1 mm and a wall thickness of 0.25 ± 0.02 mm. To compare these values with the actual material thinning that occurred, all samples were next embedded in a curing compound, cut in half, and measured under a microscope with two hundredfold magnification. The minimum wall thickness in the spin groove could thus be analyzed very precisely. The obtained results for the calculated stretched lengths L_F and L_{WC} as well as the results from the microscope measurements, are presented in Table 1. The stated values of material thinning are derived from the ratio of the

The final publication is available at Springer via
http://dx.doi.org/10.1007/978-3-032-03546-2_24

measured minimum wall thickness in the spin groove to the original wall thickness of the can. For each parameter configuration, the mean value is calculated from the 10 available samples of that configuration.

Table 1. Results of the experiments conducted for the evaluation of the proposed methodology.

Parameter Configuration	A	B	C	D	E	F
Calculated Stretched Length L_F in mm	74.292	74.742	74,991	75.369	75.796	76.211
ΔL $(= L_F - L_{original})$ in mm	1.292	1.742	1.991	2.369	2.796	3.211
Calculated Stretched Length L_{WC} in mm	6.666	7.335	7.475	8.081	8.643	9.230
Measured Material Thinning MT in %	17.7	27.9	29.7	32.2	32.4	41.4

The difference ΔL between the calculated stretched length L_F and the actual length $L_{original}$ in comparison with the values of the occurring material thinning is depicted in Fig. 2(a). Fig. 2(b) shows the relation between the calculated stretched length L_{WC} and the occurring material thinning.

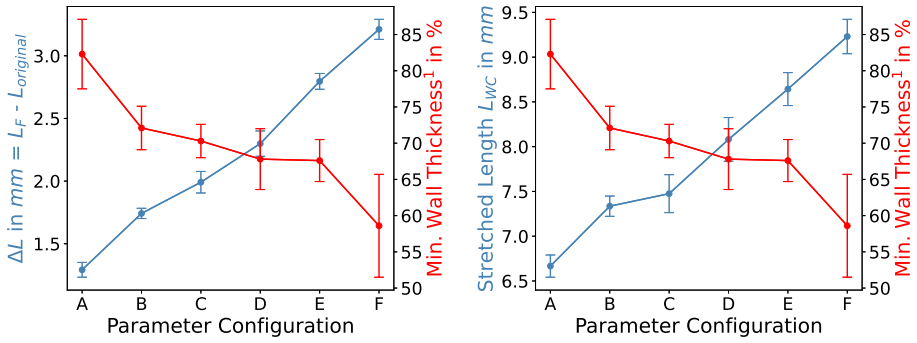

(a) ΔL and Wall Thickness (b) L_{WC} and Wall Thickness

Fig. 2. Comparison of the calculated stretched lengths with the measured wall thickness. ([1] = Original Wall Thickness − Material Thinning MT)

From the diagrams, the relationship between the calculated length difference ΔL and wall thickness, as well as between the reduced stretched length L_{WC} and wall thickness, is clearly visible. However, for the measured minimal wall thickness, the standard deviation of the parameter configurations, indicated by the vertical error bars, varies significantly. This variation in results can be attributed to the multiple manual process steps performed by different staff members to obtain the cross-sectional images, including embedding, cutting, polishing, and measuring the probes. The particularly high standard deviation of Configuration F can be attributed to the critically low wall thickness of the cell cans in this

The final publication is available at Springer via
http://dx.doi.org/10.1007/978-3-032-03546-2_24

configuration, which results in drastic material thinning and, consequently, a greater variation in the measured wall thicknesses. Taking these factors into account, it can be hypothesized that the material thinning of the battery cans after spin grooving can be indirectly assessed by examining the stretched length of the entire can or even the formed bending radii. To obtain a reliable statement about the relationship between the various measured values, the Pearson correlation coefficient, referred to as R, will be calculated. This is a methodology for quantifying linear correlations between data points. The Pearson correlation coefficient ranges from -1 to 1, where 0 indicates no linear correlation, and values of 1 and -1 signify perfect positive and negative linear correlations, respectively [15]. When substituting the calculated and measured data from Table 1 into the formula for calculating the Pearson coefficient, the following calculation results emerge for $R_{\Delta L,MT}$ and $R_{L_{WC},MT}$ that refer to the depicted results in Fig. 2(a) and Fig. 2(b) [16]:

$$R_{\Delta L,MT} = \frac{6\sum_{i=A}^{F} \Delta L_i MT_i - \sum_{i=A}^{F} \Delta L_i \sum_{i=A}^{F} MT_i}{\sqrt{6\sum_{i=A}^{F} \Delta L_i^2 - (\sum_{i=A}^{F} \Delta L_i)^2}\sqrt{6\sum_{i=A}^{F} MT_i^2 - (\sum_{i=A}^{F} MT_i)^2}} = 0.9408 \quad (8)$$

$$R_{L_{WC},MT} = \frac{6\sum_{i=A}^{F} L_{WC\,i} MT_i - \sum_{i=A}^{F} L_{WC\,i} \sum_{i=A}^{F} MT_i}{\sqrt{6\sum_{i=A}^{F} L_{WC\,i}^2 - (\sum_{i=A}^{F} L_{WC\,i})^2}\sqrt{6\sum_{i=A}^{F} MT_i^2 - (\sum_{i=A}^{F} MT_i)^2}} = 0.9398 \quad (9)$$

The results $R_{\Delta L,MT} = 0.9408$ and $R_{L_{WC},MT} = 0.9398$ indicate a strong positive correlation according to the relevant literature [15]. This means that with increasing values for the calculated stretched lengths, a decreasing wall thickness in the spin groove can be expected. It can therefore be confirmed that, using our proposed calculation model, it is feasible to make a statement regarding the material thinning of the cell can. As the measurement speed of our system is designed for use in industrial mass production, its implementation can achieve a 100% inspection of the material thinning in the spin grooves of the processed battery cans. To obtain a value for any machine parameter configuration, an estimation function of material thinning $MT(L_{WC})$ can be established based on the previously recorded measurement data using the method of linear interpolation. The corresponding formula for this is:

$$MT(L_{WC}) = MT_A + \frac{(MT_F - MT_A)(L_{WC} - L_{WC,A})}{(L_{WC,F} - L_{WC,A})} \quad (10)$$

Here, MT_A and MT_F correspond to the measured material thinning of the probes of Configuration A and F, $L_{WC,A}$ and $L_{WC,F}$ refer to the corresponding calculated lengths, and L_{WC} to the inline-calculated stretched length, that is produced during the manufacturing process. This function can be implemented in the machine control system and thus serve as a process-integrated quality inspection.

To achieve the largest possible interpolation range, Parameters Configurations A and F are used for interpolation, which can be referred to as the worst-case and best-case scenarios in terms of the material thinning that occurred.

The final publication is available at Springer via
http://dx.doi.org/10.1007/978-3-032-03546-2_24

As mentioned earlier, further deterioration of the machine parameters leads to crack formation in the spin groove of the cell can. This means that by using our model, it can be checked during ongoing production whether the material thinning is within a non-critical range, thereby eliminating the risk of damaging the processed cell.

5 Conclusion and Outlook

It has been demonstrated that by calculating the stretched length of the bending radii of reshaped battery cell cans during production, a prediction can be made about the degree of material thinning in the reshaped area. However, before our proposed calculation model can be successfully implemented in production, a validation dataset consisting of cut-open battery cans must be created, which serves for the accurate measurement of the actual material thinning that occurs. Based on this data, an interpolation method can then be used to create a function of material thinning based on the measurement values from the validation dataset and the geometry measurement data that can be captured during production. Since both the software components and the camera-based measurement technology of our system are designed for use in industrial mass production, this approach enables inline monitoring of the material thinning of each processed cell. Compared to traditional methods for testing the wall thickness of battery cans, such as X-rays and CT scans, the presented methodology provides lower costs and faster cycle times, leading to reduced manufacturing scrap, lower production costs, and improved sustainability.

In future work, we plan to test the presented system in collaboration with partners from the battery cell production sector for industrial mass production. Additionally, we will explore the applicability of the methodology in other industries where high-precision metallic material forming is critical, and where material thinning may lead to significant crack formation risks.

Acknowledgments. This work was supported by a grant from the German Federal Ministry of Education and Research (BMBF) for the project "DigiBattPro 4.0" [17] under grant 03XP0374C.

Disclosure of Interests. The authors affirm that this article is original, unpublished, and not under consideration elsewhere. They have reviewed and approved the manuscript and declare no conflicts of interest.

References

1. Degen, F., Krätzig, O.: Future in battery production: An extensive benchmarking of novel production technologies as guidance for decision making in engineering. IEEE Transactions on Engineering Management **71**, 1038–1056 (2024). https://doi.org/10.1109/TEM.2022.3144882

The final publication is available at Springer via http://dx.doi.org/10.1007/978-3-032-03546-2_24

2. Baazouzi, S., Feistel, N., Wanner, J., Landwehr, I., Fill, A., Birke, K.P.: Design, properties, and manufacturing of cylindrical li-ion battery cells—a generic overview. Batteries **9**(6), 309 (2023). https://doi.org/10.3390/batteries9060309
3. Pegel, H., Jany, L., Sauer, D.U.: Pareto–optimal design of automotive battery systems with tabless cylindrical lithium–ion cells: Resolving the trade–off between energy, performance, weight, and cost for variable vehicle requirements. Energy Technology (2024). https://doi.org/10.1002/ente.202401479
4. Link, S., et al.: Development perspectives for lithium-ion battery cell formats (2022), https://www.isi.fraunhofer.de/en/blog/themen/batterie-update/lithium-ionen-batteriezellen-entwicklung-batteriezellformate.html
5. Yu, L., Bai, Y., Polzin, B., Belharouak, I.: Unlocking the value of recycling scrap from li-ion battery manufacturing: Challenges and outlook. Journal of Power Sources **593**, 233955 (2024). https://doi.org/10.1016/j.jpowsour.2023.233955
6. Rangarajan, S., Sunddararaj, S.P., Sudhakar, A.V., Shiva, C.K., Subramaniam, U., Collins, E.R., Senjyu, T.: Lithium-ion batteries—the crux of electric vehicles with opportunities and challenges. Clean Technologies **4**(4), 908–930 (2022). https://doi.org/10.3390/cleantechnol4040056
7. Quinn, A., Darst, J., Keyser, M., Coman, P.T., Barrera, T.P., Shearing, P.R., Petrushenko, D., Finegan, D.P., Darcy, E.: Achieving passive thermal runaway propagation resistance in li-ion battery packs. The Electrochemical Society Interface **33**(3), 55 (2024). https://doi.org/10.1149/2.F08243IF
8. Masuch, S., Gümbel, P., Kaden, N., Dröder, K.: Applications and development of x-ray inspection techniques in battery cell production. Processes **11**(1), 10 (2022). https://doi.org/10.3390/pr11010010
9. Jiang, Y., Tian, A., Yan, L., Du, X., Yang, L., Li, L., Zhou, J., Wang, Q., Ruan, S., He, X., Zhang, Y., Yu, X., Jiang, Y., Tu, F., Xiang, J., Wan, W., Wang, C., Xia, Y., Xia, X., Zhang, W.: X-ray computed tomography (ct) technology for detecting battery defects and revealing failure mechanisms. Journal of Electronic Materials **53**(10), 5776–5787 (2024). https://doi.org/10.1007/s11664-024-11300-9
10. Zoesch, A., Wiener, T., Kuhl, M.: Zero defect manufacturing: Detection of cracks and thinning of material during deep drawing processes. Procedia CIRP **33**, 179–184 (2015). https://doi.org/10.1016/j.procir.2015.06.033
11. Schwenke, H., Neuschaefer-Rube, U., Pfeifer, T., Kunzmann, H.: Optical methods for dimensional metrology in production engineering. CIRP Annals **51**(2), 685–699 (2002). https://doi.org/10.1016/S0007-8506(07)61707-7
12. Telecentric measurement system - tm-x5000 series: Silhouette-based analysis for guaranteed accuracy (2025), https://www.keyence.com/products/measure/micrometer/tm-x5000/
13. Fischer, U., Gomeringer, R., Heinzler, M., Kilgus, R., Näher, F., Oesterle, S., Paetzold, H., Stephan, A.: Mechanical and Metal Trades Handbook. Textbook series from Europa-Lehrmittel for the metalworking trades, Verlag Europa-Lehrmittel Nourney Vollmer GmbH & Co. KG, Haan-Gruiten, Germany, 4th english edition edn. (2018), https://www.europa-lehrmittel.de/Mechanical-and-Metal-Trades-Handbook/1910X-4
14. Kong, Q., Siauw, T., Bayen, A.M. (eds.): Python Programming and Numerical Methods: A Guide for Engineers and Scientists. Academic Press (2021), https://www.sciencedirect.com/book/9780128195499/python-programming-and-numerical-methods
15. Akoglu, H.: User's guide to correlation coefficients. Turkish journal of emergency medicine **18**(3), 91–93 (2018). https://doi.org/10.1016/j.tjem.2018.08.001, https://www.sciencedirect.com/science/article/pii/S2452247318302164

The final publication is available at Springer via http://dx.doi.org/10.1007/978-3-032-03546-2_24

16. Baldi, P., Brunak, S., Chauvin, Y., Andersen, C.A., Nielsen, H.: Assessing the accuracy of prediction algorithms for classification: an overview. Bioinformatics **16**(5), 412–424 (2000). https://doi.org/10.1093/bioinformatics/16.5.412
17. Fraunhofer Institute for Manufacturing Engineering and Automation IPA: Project "digibattpro 4.0"–digitalisierte batteriezellproduktion 4.0: founded by the german federal ministry of education and research (bmbf) (03042025), https://www.ipa.fraunhofer.de/de/referenzprojekte/DigiBattPro40-BMBF.html

The final publication is available at Springer via http://dx.doi.org/10.1007/978-3-032-03546-2_24